Recombination of Methyl Radicals. 1. New Data between 1175 and 1750 K in the Falloff Region†

Hong Du‡ and Jan P. Hessler*

Gas Phase Chemical Dynamics Group, Chemistry Division, Argonne National Laboratory, 9700 South Cass Avenue, Argonne, Illinois 60439

Paul J. Ogren

Department of Chemistry, Earlham College, Richmond, Indiana 47374

Received: May 2, 1995; In Final Form: August 21, 1995⊗

The rate coefficient for the recombination of methyl radicals, $CH_3 + CH_3 \rightarrow C_2H_6$, was measured in incident shock-wave experiments on azomethane (0.12−1.3%) in argon. Methyl radicals were detected at 46 294 cm^{-1} (215.94 nm in air) by the tunable-laser flash-absorption technique. Postshock pressures between 114 and 230 kPa (1.13−2.27 atm) produced buffer gas concentrations between 5.4×10^{18} and 1.1×10^{19} cm^{-3}. The cross section for optical absorption, the rate of dissociation of azomethane, and the rate coefficient of the recombinational reaction were determined simultaneously by least-squares analysis of methyl absorption profiles. The rate coefficient for the dissociation of azomethane from 850 to 1430 K is $k_{dis}(T) = 2.22 \times 10^{39} T^{-7.99} \exp\{-25920/T(\mathrm{K})\}$ s^{-1}. The temperature-dependent rate of recombination at 1.2 atm compares favorably with previous measurements. In terms of the phenomenological three-parameter equation of Kooji and the asymmetric Lorentzian broadening function of Gilbert et al., the recombination data from 296 to 1800 K may be described by $k_\infty(T) = 1.53 \times 10^{-7} T^{-1.203} \exp\{-295/T(\mathrm{K})\}$ $cm^3 s^{-1}$, $k_0(T) = 1.70 \times 10^{-5} T^{-7.248} \exp\{-2172/T(\mathrm{K})\}$ cm^6 s^{-1}, and $F_{cent}(T) = \exp\{-T(\mathrm{K})/506\}$.

I. Introduction

The recombinational reaction of the methyl radical to form ethane is of considerable interest to experimental and theoretical kineticists as well as modelers of combustion processes. This reaction is a major termination reaction in the pyrolysis and oxidation of hydrocarbons,[1,2] is frequently used as a reference in kinetic studies,[3] and is a benchmark for testing and improving statistical theories.[4,5] Below 1000 K the NIST Data Base[6] contains over 40 references to early investigations. More recent measurements[7−9] provide a fairly complete description of the low-temperature behavior. Above 1000 K, experimental information is relatively scarce. Clark et al.[10] studied the reaction at number densities of 9×10^{17} cm^{-3} between 1120 and 1400 K with mass spectrometry in a single-pulse shock tube. Similarly, Held et al.[11] studied the reaction in a flow reactor at pressures between 10 and 80 Torr and 1005 K via optical absorption and gas chromatography. Glänzer et al.[12,13] were the first to employ optical absorption by the methyl radical[14,15] at the high temperatures produced by shock tubes. Hwang et al.[16] have also studied methyl−methyl recombination up to 1650 K and near the high-pressure limit. Zaslonko and Smirnov[17] used optical absorption to study the reaction at 1740 K near atmospheric pressure, and Hwang et al.[18] have studied it between 1300 and 1700 K in the falloff region near atmospheric pressure. In this paper, we report results of individual measurements of the rate of methyl−methyl recombination, the cross section for optical absorption by the methyl radical, and the rate of dissociation of azomethane over the temperature range 1175−1750 K and the pressure range 114−230 kPa (1.13−2.27 atm). We also present phenomenological equations which describe the recombinational reaction over the complete temperature and pressure range of all experiments. These equations may be used to model the combustion process. In a subsequent paper,[19] we develop a criterion for selecting and correcting data, combine the data presented here with previous measurements, demonstrate that the temperature dependence of the high-pressure rate coefficient may be described by a simple exponential function, and perform a series of global fits with different descriptions for the pressure-dependent behavior of the rate in the falloff region.

Section II of this paper provides a brief description of our experimental technique and apparatus. In section III, we discuss the reaction mechanism used to model our absorption profiles. A unique feature of this mechanism is the inclusion of independent descriptions of singlet and triplet methylene chemistry. Sensitivity calculations are used to show that, under our experimental conditions, the cross section for optical absorption and the rates of the reactions must be determined simultaneously. In section IV, we present our results: the cross section for optical absorption, the rate of dissociation of azomethane, and the rate of methyl−methyl recombination. As part of the discussion in section V, we combine our measured rate of dissociation of azomethane with the lower temperature measurements of Glänzer et al. and conclude that the data are consistent with either a concerted or sequential mechanism for dissociation. A set of phenomenological equations is presented which describes the experimental results. The rate coefficients reported here compare favorably with previous measurements and extend the data base for this reaction.

II. Experimental Section

Azomethane was made using the procedure of Renaud and Leitch.[20] It was purified by bulb-to-bulb distillation immediately

† Work performed under the auspices of the U.S. Department of Energy, Office of Basic Energy Sciences, Division of Chemical Sciences, under Contract No. W-31-109-Eng-38.

‡ Present address: Texas Instruments, P.O. Box 650311, Dallas, TX 75265.

* To whom correspondence should be addressed.

⊗ Abstract published in *Advance ACS Abstracts,* December 15, 1995.

0022-3654/96/20100-0974$12.00/0

after production and before the preparation of samples. The diluent, argon, was purchased from Airco; impurities were O_2, CO, CO_2, total hydrocarbons, and H_2O all <1 ppm, H_2 <2 ppm, and N_2 <4 ppm. Further purification was not attempted. Samples were prepared by the partial pressure method in a baked, electro-polished, 3-L, stainless-steel vessel. The purities of every batch of azomethane and the final samples were checked with a magnetic-sector mass spectrometer. These analyses indicated that other hydrocarbons were not present, that the only detectable impurity was carbon dioxide at 0.011% (volume), and that azomethane did not adhere to the walls of our apparatus.

A 2.0-m long, honed, electro-polished, stainless steel shock tube with an inner diameter of 25.4 mm was used to produce the high temperatures.[21] Several Mylar diaphragms (0.03 mm thick) separated the expansion section from the drive section. The drive gas was 99.999% helium. Prior to each experiment the expansion section was evacuated to less than 2.0×10^{-6} Torr with a turbo-molecular pump equipped with magnetic-levitation bearings. Samples were introduced into the experimental section from the end of the shock tube nearer the detector. A capacitance manometer was used to measure the initial pressure in the tube and a thermocouple measured the initial temperature. The uncertainty in the pressure readings is $\pm$(0.15% + 0.005 Torr), and the uncertainty in the initial temperature is $\pm$0.5 K. To produce a shock wave, helium was introduced quickly into the drive section. The velocity of the shock wave was measured with six barium titanate piezoelectric transducers mounted at 100-mm intervals along the expansion section. The time intervals between these transducers were measured with a 10 MHz clock and were least-squares fit to a quadratic equation. The root-mean-squared deviation of this fit was used to estimate the uncertainty in the shock speed. In general, this uncertainty is less than 0.2% at the 2σ (95.4%) confidence level. Over the interval of the absorption profile, approximately 25 mm, the velocity of the shock front is constant to within 1 part in 10^3. Because we are probing only a short distance behind the shock front, less than 25 mm, boundary layer corrections[22] were calculated to be unnecessary.

The temporal dependence of the concentration of methyl radicals was monitored behind incident shock fronts with the tunable-laser flash-absorption technique.[23] The wavelength of the fundamental light was determined by a $^1/_2$-m spectrometer and set at 431.9 $\pm$ 0.1 nm (air). The time-averaged band width of the light from the dye laser was 0.02 cm^{-1}. A β-barium-borate crystal was used to generate the second harmonic of the fundamental light and a constant-deviation prism separated the two beams. The wavenumber of the doubled light was 46 294 $\pm$ 11 cm^{-1} (vacuum); this corresponds to a wavelength of 215.94 $\pm$ 0.05 nm (air) and coincides with the absorption maximum for the R-branch transitions[24] between the B($^2A'_1$) and X($^2A''_2$) electronic states of methyl. To remove any fluorescence from the sample, a narrow band-pass filter was used between the exit window of the shock tube and the detector. The absorption profile obtained at our highest temperature, 1742 K, is shown in Figure 1. The data in front of the shock wave are used to normalize the pulse-to-pulse energy fluctuations of the light. The noise in this signal is on the order of 2 m^{-1}. The small negative and large positive spike between 0 and 0.2 μs is due to diffraction by the curved shock front. A discussion of the useful kinetic information contained in this profile will be presented in the next section.

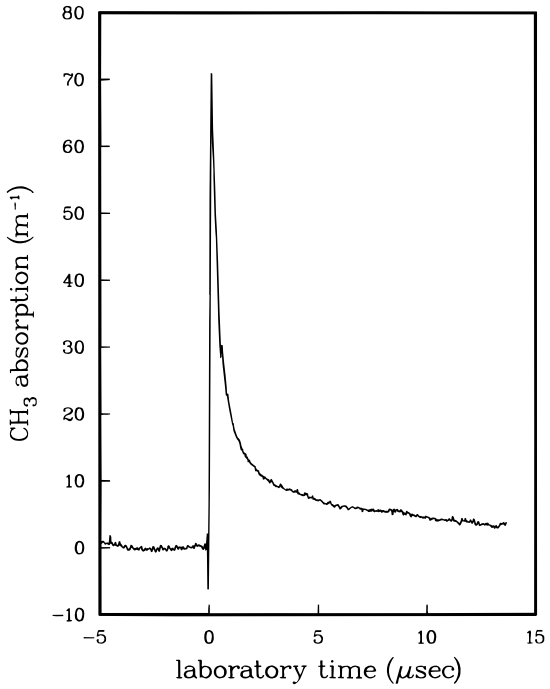

Figure 1. Absorption profile of the methyl radical. Initial conditions: 1.28% azomethane in argon, P_1 = 8.02 kPa, T_1 = 293.0 K, U_{shock} = 1.322 km/s. The sharp spike just behind t = 0 is due to diffraction of the light by the curved shock front.

III. Experimental Design and Method of Data Reduction

A. Reaction Mechanism. The reaction mechanism used for this study is shown in Table 1. This mechanism contains 14 species, and all of the reactions in the mechanisms of Hwang et al.[18] and Davidson et al.[25] In addition, we include separate descriptions of the chemical reactivity of singlet and triplet methylene. Our mechanism is comparable to the mechanism for the combustion of methane presented by Frenklach et al.[26] Our mechanism does not contain any C_3 species, the methyne radical, or the C_2H radical. Most of the values for the rate coefficients come from the recent review by Baulch et al.,[27] the earlier review by Tsang and Hampson,[28] or the NIST Chemical Kinetics Database.[6] To obtain up-to-date values, we have consulted the review by Michael and Lim.[29] The thermodynamic properties of the species of a mechanism are just as important as the parameters for the rate coefficients. We use the CHEMKIN Thermodynamic Data Base.[30] In this database the thermodynamic properties of the methyl radical were calculated in 1969. Similarly, the properties of ethane are based upon calculations performed in 1977. More recent calculations of the thermodynamic properties of the methyl radical, ethane, and azomethane were reported in 1982.[31] Since 1982, the heat of formation of the methyl radical has been remeasured.[32,33] A weighted average of these two results gives $\Delta H_f(CH_3)$ = 146.59 $\pm$ 0.40 kJ·mol^{-1}. We use the heat of formation obtained by Pamidimukkala et al. since it falls within the uncertainty of the more recent results. The major influence of these new properties will be reflected in calculations of the equilibrium constant for reaction 8. For example, at a pressure of 1 atm and 1200 K the ratio of the new-to-old equilibrium constant for the methyl−methyl recombination reaction is 1.40. At 1800 K this ratio is 1.32. Therefore, the calculated rate of dissociation of ethane will be reduced between 32 and 40% when we go from the original CHEMKIN Thermodynamic Data Base to the newer thermodynamic properties for ethane and the methyl radical. Below, we discuss the unique features of our mechanism.

Methyl−Methyl Recombination. Basically, this reaction has five channels: reactions 8−11, and the inverse of reaction 28. Reaction 8 is the subject of this paper and, for the purposes of evaluation, is treated as a simple bimolecular reaction. The high

TABLE 1: Reaction Mechanism for Simple Hydrocarbons

no.	reaction	A ($cm^3\ s^{-1}$)	β	$\Delta E/k$ (K)	ref
	Reactions of Hydrogen				
1.	$H_2 + M \leftrightarrow 2H + M$ (H_2 enhanced by 4.0)	3.7E−10	0.0	48350	27, p 550
	Reactions of Methane				
2.	$CH_4(+M) \leftrightarrow CH_3 + H(+M)$	2.4E+16	0.0	52800	27, p 673
	low-pressure limit	1.2E−06	0.0	47000	
	TROE centering 0.362 3231 1.0				
3.	$CH_4 + H \leftrightarrow CH_3 + H_2$	2.2E−20	3.0	4050	27, p 516
	Reactions of Ethane				
4.	$C_2H_6 + H \leftrightarrow C_2H_5 + H_2$	2.4E−15	1.5	3730	27, p 533
	Reactions of the Methyl Radical				
5.	$CH_3 + M \leftrightarrow (T)CH_2 + H + M$	1.7E−08	0.0	45600	27, p 648
6.	$CH_3 + H \leftrightarrow (S)CH_2 + H_2$	1.0E−10	0.0	7600	27, p 511
7.	$CH_3 + C_2H_6 \leftrightarrow C_2H_5 + CH_4$	2.5E−31	6.0	3040	27, p 668
8.	$CH_3 + CH_3(+M) \leftrightarrow C_2H_6(+M)$	1.53E−07	−1.203	295	this work and ref 19
	low-pressure limit	1.7E−05	−7.248	2172	
	TROE centering 0.0 506 1.0				
9.	$CH_3 + CH_3 \leftrightarrow C_2H_5 + H$	5.3E−11	0.0	7384	35
10.	$CH_3 + CH_3 \leftrightarrow C_2H_4 + H_2$	1.7E−10	0.0	16103	40
11.	$CH_3 + CH_3 \leftrightarrow CH_4 + (T)CH_2$	1.7E−12	0.0	6992	see text
	Reactions of the Ethyl Radical				
12.	$C_2H_5(+M) \leftrightarrow C_2H_4 + H(+M)$	1.1E+10	1.0	18500	45
	low-pressure limit	6.6E+09	−5.0	20130	
	TROE centering 0.194 1350 1.0 3100 see text				
13.	$C_2H_5 + H \leftrightarrow C_2H_4 + H_2$	3.0E−12	0.0	0	28, p 1174
14.	$C_2H_5 + CH_3 \leftrightarrow CH_4 + C_2H_4$	1.9E−12	0.0	0	27, p 665
15.	$C_2H_5 + C_2H_5 \leftrightarrow C_2H_4 + C_2H_6$	2.4E−12	0.0	0	27, p 707
	Reactions of Ethylene				
16.	$C_2H_4 + M \leftrightarrow C_2H_2 + H_2 + M$	1.8E+17	−6.6	47560	6
17.	$C_2H_4 + M \leftrightarrow C_2H_3 + H + M$	6.3E−07	0.0	49400	28, p 1182
	H_2 enhanced by 2.9				
	N_2 enhanced by 1.2				
18.	$C_2H_4 + H \leftrightarrow C_2H_3 + H_2$	2.2E−18	2.5	6160	28, p 1185
19.	$C_2H_4 + CH_3 \leftrightarrow C_2H_3 + CH_4$	6.9E−12	0.0	5600	27, p 663
20.	$C_2H_4 + C_2H_5 \leftrightarrow C_2H_6 + C_2H_3$	1.1E−21	3.13	9060	28, p 1191
	Reactions of the Vinyl Radical				
21.	$C_2H_3(+M) \leftrightarrow C_2H_2 + H(+M)$	2.0E+14	0.0	20000	27, p 704
	low-pressure limit	6.9E+17	−7.5	22900	
	TROE centering 0.350 1.0 1.00E+06				
22.	$C_2H_3 + H \leftrightarrow C_2H_2 + H_2$	2.0E−11	0.0	0	27, p 528
23.	$C_2H_3 + CH_3 \leftrightarrow C_2H_2 + CH_4$	6.5E−13	0.0	0	28, p 1202
24.	$C_2H_3 + C_2H_5 \leftrightarrow C_2H_4 + C_2H_4$	8.0E−13	0.0	0	28, p 1202
25.	$C_2H_3 + C_2H_5 \leftrightarrow C_2H_2 + C_2H_6$	8.0E−13	0.0	0	28, p 1202
26.	$C_2H_3 + C_2H_3 \leftrightarrow C_2H_4 + C_2H_2$	1.6E−12	0.0	0	28, p 1204
	Reactions of the Singlet-Methylene Radical				
27.	$(S)CH_2 + M \leftrightarrow (T)CH_2 + M$	6.0E−12	0.0	0	27, p 644
	H enhanced by 55.0				
	N_2 enhanced by 1.7				
	CH_4 enhanced by 2.0				
	C_2H_2 enhanced by 13.3				
	C_2H_4 enhanced by 3.8				
	C_2H_6 enhanced by 6.0				
28.	$(S)CH_2 + CH_4 \leftrightarrow CH_3 + CH_3$	7.1E−11	0.0	0	28, p 1256
29.	$(S)CH_2 + C_2H_6 \leftrightarrow C_2H_5 + CH_3$	1.9E−10	0.0	0	28, p 1257
30.	$(S)CH_2 + CH_3 \leftrightarrow C_2H_4 + H$	3.0E−11	0.0	0	28, p 1260
31.	$(S)CH_2 + C_2H_5 \leftrightarrow C_2H_4 + CH_3$	1.5E−11	0.0	0	28, p 1260
32.	$(S)CH_2 + C_2H_3 \leftrightarrow C_2H_2 + CH_3$	3.0E−11	0.0	0	28, p 1261
33.	$(S)CH_2 + (S)CH_2 \leftrightarrow C_2H_2 + H_2$	2.0E−11	0.0	400	28, p 1260
34.	$(S)CH_2 + (S)CH_2 \leftrightarrow C_2H_2 + H + H$	1.8E−10	0.0	400	28, p 1260
	Reactions of the Triplet-Methylene Radical				
35.	$(T)CH_2 + CH_3 \leftrightarrow C_2H_4 + H$	7.0E−11	0.0	0	27, p 641
36.	$(T)CH_2 + C_2H_5 \leftrightarrow CH_3 + C_2H_4$	3.0E−11	0.0	0	27, p 1269
37.	$(T)CH_2 + C_2H_3 \leftrightarrow CH_3 + C_2H_2$	3.0E−11	0.0	0	27, p 1270
38.	$(T)CH_2 + (S)CH_2 \leftrightarrow C_2H_2 + H_2$	3.0E−11	0.0	0	27, p 1272
39.	$(T)CH_2 + (T)CH_2 \leftrightarrow C_2H_2 + H_2$	2.0E−11	0.0	400	27, p 640
40.	$(T)CH_2 + (T)CH_2 \leftrightarrow C_2H_2 + H + H$	1.8E−10	0.0	400	27, p 640
	Dissociation of Azomethane				
41.	$C_2H_6N_2 \rightarrow CH_3 + CH_3 + N_2$	2.2E+39	−7.99	25920	this work

sensitivity of atomic resonance absorption spectophotometry[34] has allowed reaction 9 to be studied under ideal conditions. Measurements of the rate coefficient for this reaction have recently been extended by Lim and Michael,[35] who confirm the results obtained by Frank[36] and Frank and Braun-Unkhoff[37] between 1320 and 2300 K. Therefore, we assume the rate coefficient of reaction 9 is known to within 25%. The rate coefficient for reaction 10 is controversial. Baulch et al. state there are insufficient data to make a recommendation, Tsang and Hampson do not discuss it, and Frenklach et al. explicitly exclude it. The early works[36,38,39] give nearly identical results with a bimolecular $k(T) \sim 6.5 \times 10^{-9} \exp\{-15430/T(\mathrm{K})\}$ cm^3 s^{-1}. The latest work by Hidaka et al.[40] gives a much lower value of $1.7 \times 10^{-10} \exp\{-16103/T(\mathrm{K})\}$ cm^3 s^{-1}. Gordon et al.[41] have calculated the transition state and obtain a barrier of 136 kJ/mol or $\Delta E/k \approx 16\,400$ K. They conclude, "the concerted elimination of molecular hydrogen to form ethylene appears to be a very unlikely process". Therefore, we use the lower value of Hidaka et al. Consequently, at the highest temperature of our measurements, 1742 K, the ratio of the rate for atomic-to-molecular elimination, k_9/k_{10}, will be 4500:1. Had we used the earlier rate expression this ratio would be near 1:1. The situation with respect to reaction 11 is, at best, tenuous. The only available experimental information comes from the rate of the reverse reaction measured by laser magnetic resonance from 296 to 707 K by Böhland et al.[42] They state that their results "are not sufficiently accurate to determine Arrhenius parameters from this measurement". To obtain an Arrhenius expression they assume the preexponential factor per bond is the same as that of ethane and conclude $k_{-11}(T) = 7.13 \times 10^{-12} \exp\{-5052/T(\mathrm{K})\}$ cm^3 s^{-1}. We estimate the uncertainty in this expression to be at least a factor of 10 at 1000 K. Despite this, we use this expression, along with the more recent thermodynamic properties of the methyl radical, to calculate the equilibrium constant and rate coefficient for reaction 11. Frank and Braun-Unkhoff[36] used the same approach. However, they found curvature in the Arrhenius expression. The ratio of the rate of production of atomic hydrogen-to-triplet methylene is between 250:1 and 2.5:1 at 1750 K. With regard to the reverse of reaction 28, several measurements at room temperature[28] give the total rate coefficient for removal of singlet methylene by methane at 7×10^{-11} cm^3 s^{-1}. Laser magnetic resonance measurements of the rate of intersystem crossing[43] show that this reaction dominates deactivation by a ratio of 6:1. We assume the coefficient for reaction is temperature independent and, from a similar calculation of the equilibrium constant, obtain a value for k_{-28} of 1.7×10^{-13} cm^3 s^{-1} at 1750 K. At this rate, the ratio of the rate of production of atomic hydrogen-to-singlet methylene is only 4.5:1. Under combustion conditions, the rapid deactivation of singlet-to-triplet methylene will keep the concentration of singlet methylene low. However, the reverse of reaction 28 represents a significant channel for the removal of methyl radicals at temperatures greater than 1800 K.

Dissociation of the Ethyl Radical. Recently, Hanning-Lee et al.[44] and Feng et al.[45] have studied the decomposition of the ethyl radical, the reverse reaction, and the enthalpy of formation of the ethyl radical. Feng et al. have combined their results with previous results to obtain modified Arrhenius expressions for the rate coefficient in the high- and low-pressure limits as well as the coefficients in the modification of the Lindemann-Hinshelwood expression introduced by Gilbert et al.[46] Their expressions are valid from 200 to 1100 K. To obtain expressions at higher temperatures we used the RRKM calculations presented by Tsang and Hampson[28] to calculate the rate coefficient in the low-pressure limit and the Troe centering parameter, F_c, for each temperature of the RRKM calculation. From a comparison of these calculations with the results of Feng et al. we conclude that the rate coefficients of Feng et al. may be extrapolated to 2500 K. Our results for F_c agree with those of Feng et al. below 1100 K. However, above 1100 K they reach a minimum and then begin to increase with temperature. Therefore, we use the four-parameter description for F_c given in the mechanism.

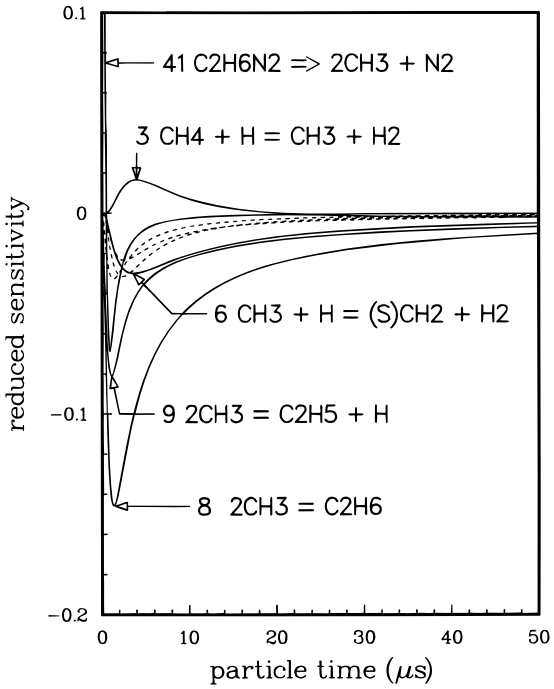

Figure 2. Reduced sensitivity coefficients for methyl at the frozen shock conditions of the profile in Figure 1: 1.28% azomethane in argon, $P_2 = 177$ kPa, and $T_2 = 1742$ K. Only 8 of the 41 reactions of the mechanism have significant sensitivity. The sensitivities for reactions 2, 12, and 28 are shown as the dashed lines.

Dissociation of Azomethane. For sensitivity calculations we used the expression from Möller et al.[47]

B. Sensitivity and Correlation Analysis. Now that we have established the reaction mechanism, we use it to design the approach for performing experiments and analyzing their results. The reduced sensitivity coefficients for methyl with respect to the rates of each reaction are defined[48] as $\{k_i/[\mathrm{CH_3}]_{\max}\}\, \partial[\mathrm{CH_3}(t)]/\partial k_i$ where the subscript i identifies the reaction, the maximum concentration of methyl is $[\mathrm{CH_3}]_{\max}$, and the time-dependent methyl concentration is $[\mathrm{CH_3}(t)]$. The reduced sensitivity coefficient with respect to the cross section for optical absorption is given by $[\mathrm{CH_3}(t)]/[\mathrm{CH_3}]_{\max}$ and varies between 0 and 1. The derivation of this result and a discussion of methyl−methyl recombination at 1300 K have been published.[49] Here, we analyze our highest temperature measurement at 1742 K and discuss the influence of secondary reactions. Plots of the reduced sensitivity coefficients[50] as a function of time are shown in Figure 2. The reduced sensitivity coefficient with respect to the cross section reaches a peak of 1.0 near 0.4 μs and is proportional to the methyl concentration. To focus this discussion on the chemistry, only the coefficients with respect to the important chemical reactions are shown in Figure 2. Inspection of a plot of the rate of destruction of the methyl radical (not shown) indicates that reactions 8 and 9 account for over 80% of the removal of methyl. Reaction 9 produces ethyl and a hydrogen atom, while the product from reaction 8, ethane, is rapidly removed by reactions 4 and 7 to give the ethyl radical,

TABLE 2: Relative Weights[a] and Correlation Coefficients[b] for the Profile of Figure 1 from the Reduced Sensitivity Coefficients of Figure 2 ($\Delta t_{particle} = 0-15$ μs)

	k_3	k_{12}	k_{28}	k_2	k_6	k_9	k_{41}	k_8	σ
k_3	0.001	0.960	0.801	0.945	0.966	0.797	0.185	0.863	−0.636
k_{12}	0.960	0.002	−0.922	−0.996	−0.970	−0.918	−0.256	−0.961	0.759
k_{28}	0.801	−0.922	0.002	−0.944	−0.827	−0.990	−0.305	−0.989	0.900
k_2	0.945	−0.996	−0.944	0.002	−0.945	−0.931	−0.274	−0.971	0.778
k_6	0.966	−0.970	−0.827	−0.945	0.004	−0.849	−0.203	−0.899	0.681
k_9	0.797	−0.918	−0.990	−0.931	−0.849	0.011	−0.276	−0.991	0.924
k_{41}	0.185	−0.256	−0.305	−0.274	−0.203	−0.276	0.017	−0.286	−0.014
k_8	0.863	−0.961	−0.989	−0.971	−0.899	−0.991	−0.286	0.046	0.883
σ	−0.636	0.759	0.900	0.778	0.681	0.924	−0.014	0.883	0.916

[a] The diagonal elements are the relative weights. [b] The off-diagonal elements are the correlation coefficients.

H_2, and methane. The ethyl radical quickly dissociates to C_2H_4 which quickly reacts with H, reaction 18, to give C_2H_3 which dissociates to produce the relatively stable species C_2H_2. To minimize the influence of these secondary reactions, we fit the absorption profile over the early time ranges where the profile decreases to between 20 and 10% of its peak value. For the example shown in Figure 2 this time range is between 6.4 and 15.0 μs. We perform a correlation analysis[51] from 0 to 15 μs to quantitatively describe the information contained in the profile of Figure 1. The results of this analysis are given in Table 2. The relative weight, or importance, of a parameter is given by the diagonal element. From this, the cross section accounts for over 90% of the information contained in the experimental profile of Figure 1. Over 99% of the kinetic information is contained in only eight reactions: 8, 41, 9, 6, 2, 28, 12, and 3. If the cross section is neglected, their respective weights are 0.543, 0.198, 0.130, 0.046, 0.029, 0.021, 0.018, and 0.009. The weight for all of the other 33 reactions totals 0.0049. Therefore, at our highest temperature over 50% of the kinetic information in the profile pertains to reaction 8. The correlation between any two parameters may be expressed in terms of the *correlation coefficient*. These range from minus to plus one and are the off-diagonal elements of Table 2. The correlation coefficient between σ and k_8 is 0.883. The correlation coefficients between k_8 and k_9, k_2, k_{28}, and k_3 are all negative and greater than 0.9. These high correlations exist because methyl−methyl recombination has important channels at this temperature, reactions 8, 9, and −28. In addition, reactions 2, 3, and 6 create or remove methyl radicals. Because of these correlations we cannot simultaneously determine k_8 and k_9 or k_8 and k_6 from the experimental profiles.

C. Data Reduction with a Dimensionless Curvature Matrix. To extract the cross section and rate coefficients from an absorption profile, we perform a nonlinear least-squares analysis to minimize the χ^2 merit function.[52] To perform this analysis, we have introduced a *dimensionless curvature matrix*[53] into the equations of standard nonlinear least-squares analysis. One advantage of this reformulation is that the dimensionless curvature matrix used to reduce the data is mathematically equivalent to the discrimination matrix of the correlation analysis discussed above. Therefore, for each experimental profile we may calculate the relative weight of each reaction and the cross section and the correlation coefficients between the varied parameters.

The analysis of an absorption profile is performed as follows. First, the diffraction spike is used to identify the origin of the shock front.[23] Second, this spike is removed from the profile by deleting points immediately after the shock front until the rate of change of the profile is comparable to the rate of change in the chemical system. Third, the reaction mechanism shown in Table 1 is used along with the initial concentrations, pressure, temperature, and shock speed to calculate the temperature, pressure, and density immediately behind the shock front. Fourth, the differential equations produced by the mechanism and the conservation laws of mass, momentum, and energy are numerically integrated to calculate the temperature, pressure, density, and concentration of each chemical species as a function of time in the particle frame. Since we are monitoring chemical changes directly behind the incident shock waves, as opposed to behind reflected shock waves, time in the laboratory frame, t_{lab}, is related to time in the moving particle frame, t_{par}, by

$$t_{lab} = \varrho_1 A_1 \int_0^{t_{par}} \frac{1}{\varrho(t')\, A(t')}\, dt' \qquad (1)$$

where the density and area across the shock tube in front of the shock front are ϱ_1 and A_1, respectively, and the density and area behind the shock front are $\varrho(t')$ and $A(t')$, respectively. The measured absorption profile, $\alpha(t_{lab})$, is calculated from

$$\alpha(t_{lab}) = \sigma(\omega,T,P)[CH_3(t_{lab})] \qquad (2)$$

where the frequency-, temperature-, and pressure-dependent cross section for optical absorption is $\sigma(\omega,T,P)$ and the concentration of the methyl radical as a function of laboratory time is $[CH_3(t_{lab})]$. These calculations are performed by converting the general-purpose computer code for predicting chemical kinetic behavior behind incident and reflected shock waves[54] into a subroutine of our nonlinear least-squares analysis code. Derivatives of the absorption profile with respect to the cross section and rate coefficients, which are needed to calculate the dimensionless curvature matrix, are calculated numerically. Once a least-squares fit is complete, the results may be used to calculate concentration profiles as a function of particle time. Examples of the methyl, ethane, methane, ethylene, and acetylene concentration profiles obtained from the fit of the absorption profile of Figure 1 are shown in Figure 3. In this example, $t_{par} \approx 3.72 t_{lab}$. To reduce the influence of secondary reactions, only data up to $t_{par} = 6.0$ μs were used to extract k_8 and the cross section. From a comparison of the long-time behavior of the observed and calculated methyl profiles of Figure 3, we may draw two significant conclusions. First, absorption by a molecular species other than methyl, for example, acetylene or ethylene, could distort the profile. This may explain the slight increase in the experimental absorption profile over the calculation. Koike and Morinaga[55] have measured the absorbtivity of these two species. At 216 nm and near 1750 K the absorption cross sections are comparable and equal to 33 pm^2. Gardiner et al.[56] have made similar measurements at 213 nm and obtain 8 pm^2 for acetylene and 33 pm^2 for ethylene. If we use the larger of the two values for acetylene and its concentration at 50 μs, we obtain an increase in absorption of only 2 m^{-1}. This is comparable to the noise in this profile and, therefore, cannot explain the slight increase in the observed profile. Second, there

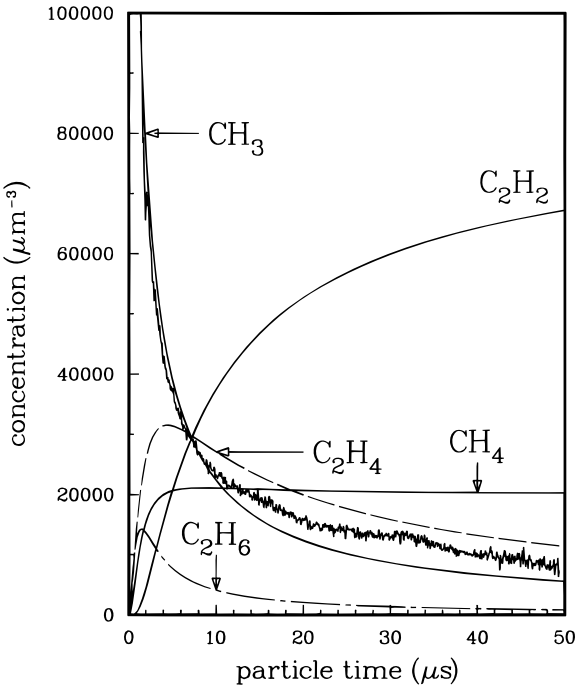

Figure 3. Calculated concentration profiles for the major carbon containing species. This calculation was performed after the least-squares analysis of the absorption profile in Figure 1. The initial methyl profile extends significantly above the figure. At the longest time shown in this figure, 50 μs, 99.9% of the carbon atoms are contained in the five species shown.

are significant uncertainties in our description of the secondary chemistry, and we can obtain a better fit of this profile if we allow one or more rate coefficients to vary. Unfortunately, the deviation between the model calculation and the measurement is not large enough to uniquely identify which reaction should be varied nor is the uncertainty assigned to the final result small enough to be meaningful. Therefore, we conclude there is no experimental evidence to suggest that our description is not adequate for the short times of these experiments. By limiting the temporal extent of the analysis to short times, we minimized the interference from other species and secondary reactions. At lower temperatures these problems are not as severe as they are at this highest temperature. In fact, the absorption profiles generally return to 0.

IV. Results

With the systematic approach discussed above, we simultaneously determined the *best-fit* values for the cross section, rate of dissociation of azomethane, and rate of methyl recombination. The *best-fit* values of the cross section are given in column 6 of Table 3 and are plotted in Figure 4 along with the results obtained by other researchers. The relative weight for the cross section, given in column 5 of Table 3, increases from 0.63 at the lowest temperature to 0.95 at the highest temperature. This trend is consistent with sensitivity and correlation analysis calculations. The random noise in the absorption profiles produces fractional uncertainties for the cross sections which range from 2 to 17% and are often below 10%. Yet, the scatter of the cross section shown in Figure 4 is closer to 20%. This disparity is endemic to measurements performed with shock tubes and has not been satisfactorily explained. Within our experimental errors the cross section is independent of pressure. To determine its temperature dependence we perform a least-squares fit to the function $A\exp\{-T(\mathrm{K})/B\}$. Over the temperature range 1175−1750 K we obtain

$$\sigma(T) = (2944^{+1469}_{-922})\exp\{-T(\mathrm{K})/(921^{+302}_{-178})\}\ \mathrm{pm}^2 \qquad (3)$$

where the uncertainties are at the 68.3% confidence level and were determined by Monte Carlo simulations. The thick solid line in Figure 4 represents eq 3. The dashed lines define the 68.3% confidence envelope.

Because the cross section plays a dominant role in determining the values of both the rate coefficient for dissociation of azomethane, k_{41}, and methyl recombination, k_8, we have reanalyzed each profile with the cross section held fixed at a value given by eq 3. This approach is analogous to the calibration procedure used in most of the previously published shock tube measurements. The results of this reanalysis are given in columns 7 and 8 of Table 3. It is important to note that in some instances both the cross section and k_8 changed significantly from the previous fit; yet, the root-mean-squared deviation remained unchanged to within 10%. This relative insensitivity of the root-mean-squared deviation is due to the

TABLE 3: Results of the Least-Squares Analysis of the Absorption Profiles

T_2 (K)	P_2 (kPa)	Δt_{lab} (μs)	signal/ noise	W_σ[a]	σ[b] (pm^2)	k_8[c] (10^{-12} cm^3 s^{-1})	k_{41}[c] (μs^{-1})
			1.28% Azomethane in Argon				
1177	145.4	1.0−10.0	35/1.7	0.63	969	7.5	0.272
						1.6	0.016
1366	238.5	0.1−14.5	70/1.9	0.71	826	6.7	1.49
						1.4	0.17
1403	246.9	0.1−7.1	70/1.8	0.76	496	6.8	1.58
						1.6	0.18
1412	231.7	0.1−7.0	65/2.1	0.75	569	6.1	1.55
						1.4	0.18
1426	223.0	0.1−14.9	70/0.87	0.78	463	6.2	1.61
						1.4	0.20
1724	174.5	0.1−4.3	75/2.7	0.93	485	1.16[d]	*e*
						0.18	
1734	175.3	0.2−3.0	65/1.1	0.94	450	0.86[d]	*e*
						0.16	
1742	177.2	0.1−6.0	70/1.4	0.95	432	0.88[d]	*e*
						0.14	
			0.447% Azomethane in Argon				
1298	144.7	0.4−7.8	30/0.46	0.73	787	5.3	0.87
						1.2	0.15
1306	136.6	0.6−7.9	25/0.56	0.71	900	6.2	0.75
						1.4	0.14
1345	131.3	0.7−11.2	20/0.28	0.72	696	5.9	0.70
						1.4	0.14
			0.105% Azomethane in Argon				
1175	158.6	1.7−10.0	9/0.25	0.78	740	5.2	0.216
						1.2	0.030
1215	147.7	0.9−12.3	8/0.38	0.73	1059	7.2	0.305
						1.6	0.048
1321	138.1	0.5−6.8	10/0.58	0.84	514	7.2	0.465
						1.7	0.075
1357	140.7	0.6−9.4	14/0.77	0.75	918	4.20	1.6
						0.69	1.2
1394	124.1	0.9−6.7	9/0.18	0.77	686	5.2	0.75
						1.5	0.37
1513	114.3	1.0−8.8	9/0.46	0.85	692	2.09	*e*
						0.64	
1537	213.0	0.3−12.2	15/1.3	0.84	540	4.00	*e*
						0.97	

[a] Relative weight of the cross section as given by the diagonal element of the dimensionless curvature matrix. [b] Value of cross section from the initial fit. [c] Rate coefficient determined with σ given by eq 3 in the text. The number below the *best-fit* value is the 68.3% confidence limit. [d] Both the cross section and k_8 were varied. [e] Above 1500 K we could not extract k_{41} from the profiles.

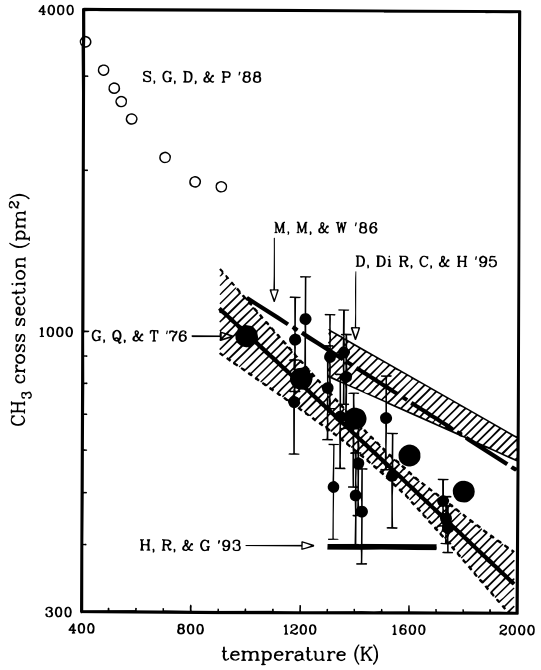

Figure 4. Cross section for optical absorption by the methyl radical at 215.94 nm (air). The solid dots with error bars are from column six of Table 3. The solid line is eq 3 and the dashed lines and shaded area define the 68.3% confidence envelope. The open circles labeled S, G, D, & P '88 are from ref. 8; the dot-dashed line labeled M, M, & W '86 is from ref 47; the five large solid points labeled G, Q, & T '76 are from refs 12 and 13; the horizontal line labeled H, R, & G '93 is from ref 18; and the shaded area labeled D, Di R, C, & H '95 is from ref 60. See the text for details.

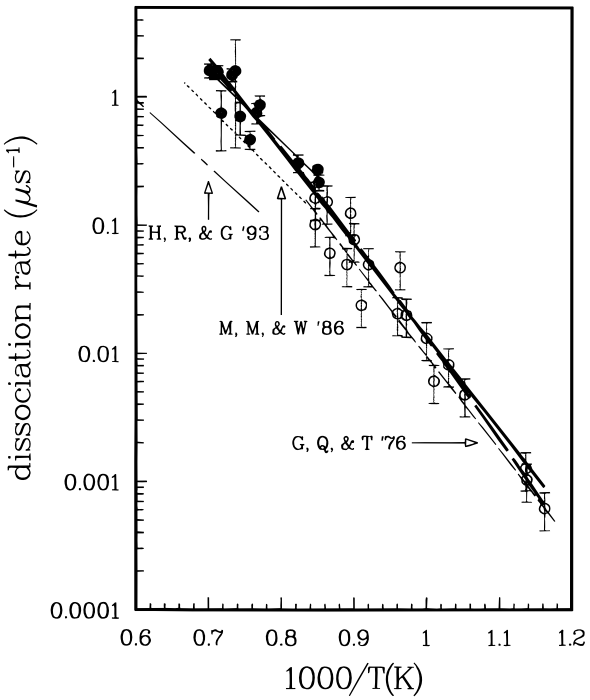

Figure 5. Rate coefficient for the dissociation of azomethane. The solid dots are from column eight of Table 3 and the error bars represent 68.3% confidence limits. The open circles are from Figure 1 of ref 12. The thick solid line from 850 to 1430 K is given by eq 7 and the thick dashed line by eq 8. The dotted line labeled M, M, & W '86 is from ref 47; the dot−dashed line labeled H, R, & G '93 is from ref 18; and the dashed line labeled G, Q, & T '76 is from ref 12. See the text for details.

high correlation between the cross section and k_8. All of the calculations performed with the cross section constrained by eq 3 fall within the noise of the experimental profile, and there is little or no indication of systematic deviations within the profiles.

Before we discuss the rate of recombination, we look at the rate of dissociation of azomethane. The results for k_{41} from Table 3 are plotted in Figure 5 along with those of previous researchers. A weighted least-squares fit of the data gives

$$\ln\{k_{41}(s^{-1})\} = (23.2 \pm 1.1) - (12693 \pm 1410)/T(K) \quad (4)$$

where the uncertainties are at the 2σ (95.4%) confidence level. Above 1500 K the rate of dissociation of azomethane was so fast we could not extract an accurate rate for the decomposition. Therefore, above 1500 K we used eq 4 to extrapolate the rate.

It is very difficult to perform a series of isobaric measurements with our shock tube system. Therefore, to display the temperature dependence of the rate coefficient for methyl−methyl recombination, we correct for the pressure-dependent shift by the prescription

$$k(T,P_{ref}) = \frac{k_{calc}(T,P_{ref})}{k_{calc}(T,P)} k(T,P) \quad (5)$$

where $k_{calc}(T,P)$ is the calculated rate coefficient at temperature T and pressure P given by Wagner and Wardlaw.[57] For convenience, we choose $P_{ref} = 122$ kPa $= 1.20$ atm. Our results are shown in Figure 6. In the paper to follow,[19] we select a set of measurements of the rate coefficient which we feel accurately describes the methyl−methyl recombination. Here, we report the results of a global fit of this set of data to the traditional temperature-dependent preexponential equation suggested by Kooji[58] and the asymmetric-Lorentzian broadening function suggested by Gilbert et al.[46] Over the temperature (296−1800 K) and pressure (0.01−50 000 kPa) ranges of the experiments the rate of methyl-methyl recombination is adequately described by

$$k_\infty(T) = 1.53 \times 10^{-7} T^{-1.203} \exp\{-295/T(K)\} \text{ cm}^3 \text{ s}^{-1} \quad (6a)$$

$$k_0(T) = 1.70 \times 10^{-5} T^{-7.248} \exp\{-2172/T(K)\} \text{ cm}^6 \text{ s}^{-1} \quad (6b)$$

$$F_{cent}(T) = \exp\{-T(K)/506\} \quad (6c)$$

The value of the reduced χ^2, χ^2/(number of degrees of freedom $= 203$) is 0.812, and the root-mean-squared deviation is 8.9×10^{-13} cm^3 s^{-1}. The parameters are highly correlated. The solid line in Figure 6 is calculated with the above equations. The shaded area around this line represents the 95.4% confidence envelope of the calculations. The Monte Carlo simulation used to calculate this confidence envelope is described in the following paper.[19] The results of other groups will be discussed in the next section.

V. Discussion

A. Cross Section for Optical Absorption. Various measurements of the cross section for optical absorption by methyl are displayed in Figure 4. For clarity, cross sections known to have been measured above 400 kPa (4 atm) have been excluded. Glänzer et al.[12,13] used a monochromator with a spectral resolution of 1.6 nm to measure the cross section between 200 and 230 nm at 1400 K. Near 216 nm they report five decadic molar extinction coefficients between 1000 and 1800 K. Möller et al.[47] used a Xe arc lamp and a monochromator to obtain a similar spectral band width, 1.6 nm. From 1000 to 2000 K and pressures between 25 and 67 kPa (0.25−0.66 atm) they

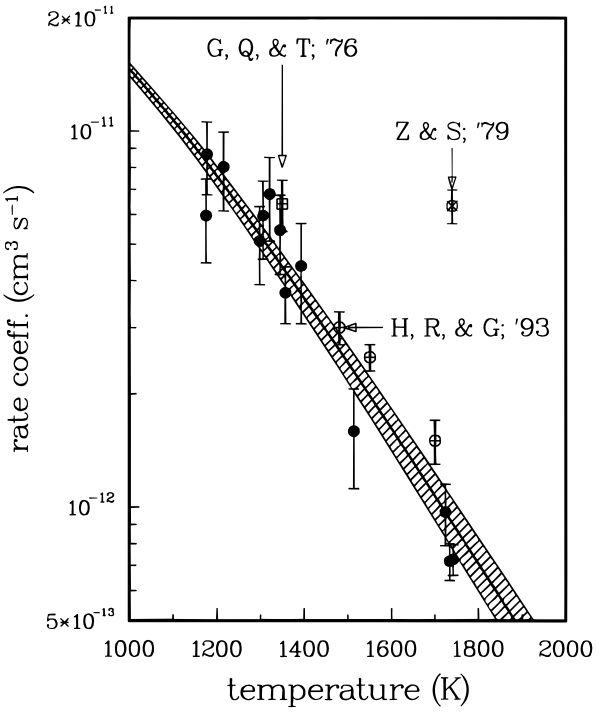

Figure 6. Rate coefficient for the recombination of methyl radicals, $CH_3 + CH_3 \rightarrow C_2H_6$ at a pressure of 122 kPa = 1.20 atm. The points are from column seven of Table 3 and corrected by eq 5 in the text. The error bars represent 68.3% confidence limits. The solid line is from the *best-fit* set of parameters given in eqs 6 and the shaded area defines the 95.4% confidence envelope. G, Q, & T '76 refers to a 1350 K datum of refs 12 and 13, Z & S '79 refers to a 1740 K datum of ref 17, and H, R, & G '93 refers to extrapolations of the 1480, 1550, and 1700 K data of ref 18. See the text for details.

obtain a cross section given by 2430 exp{$-T$(K)/1350} pm^2. This result is shown as the long/short dashed line in Figure 4. Recently, Hwang et al.[18] used a Zn arc lamp to produce 213.9 nm light. At temperatures from 1300 to 1700 K and pressures between 22 and 127 kPa (0.2 and 1.3 atm) they obtained a temperature- and pressure-independent decadic molar extinction coefficient of (1.04 ± 0.13) × 10^6 cm^2 mol^{-1}, which gives a cross section of 400 ± 50 pm^2. The cross section is shown as the thick horizontal line in Figure 4. To compare this cross section with measurements performed at 216 nm, one should multiply these results by a factor of 2. The low-temperature absorption measurements[8] were performed with a Xe arc lamp and monochromator to generate 216.36 nm light with a bandwidth of 0.6 nm. Their cross sections vary systematically and are shown as the open circles in Figure 4. Between 296 and 577 K these cross sections were found to be pressure independent up to 53 kPa (0.53 atm). The cross sections reported at 700, 810, and 906 K appear to be high. We will discuss these in detail in our subsequent paper.[19] Davidson et al.[59] used a continuous-wave dye laser and a β-barium borate crystal to produce 216.615 nm (air) light with a spectral width of less than 30 MHz (5 × 10^{-6} nm). Between 1350 and 2400 K and over the pressure range 60−142 kPa (0.6−1.4 atm) they reported a pressure independent absorption cross section given by 7666 exp{$-T$(K)/1087} pm^2. Recently, they discovered a problem with their mixing protocol and reevaluated their results.[60] This newer result, 2000 exp{$-T$(K)/1675}, along with a 20% uncertainty at 1300 K and a 10% uncertainty at 2000 K is shown as the shaded area in Figure 4. From this figure we conclude that cross sections measured in different laboratories agree to within their respective experimental uncertainties below 1500 K. Above 1500 K the results diverge. We note that the low temperature data of Slagle et al. suggest a steeper slope for the temperature dependent behavior than that proposed by Davidson et al. Differences in the central wavelength and bandwidth of the instruments used to perform the measurements could account for these differences.

B. Rate of Dissociation of Azomethane. All of the previously measured rates of dissociation of azomethane are shown in Figure 5. The lower temperature measurements of Glänzer et al. were obtained by absorption measurements both on azomethane and the methyl radical. The work of Möller et al. is based only on methyl absorption and has very large experimental uncertainties. We consider these two results to be in agreement with our results. Our slightly higher values may be simply due to the higher dynamic range of our detection system. The results of Hwang et al. are low by a factor of 2 and not within our experimental errors. Recall, their temporal signal is convoluted by the finite width (∼1.9 mm) of their light beam. They have tried to compensate for this; however, accurate compensation is only possible when the signal-to-noise ratio is very high.[61,62] Therefore, their low value for the rate of dissociation of azomethane may simply be due to the low effective dynamic range of their detection system.

When we combine the lower temperature data of Glänzer et al., 850−1200 K, with our data, 1175−1426 K, the entire set can be fit by the equation

$$\ln\{k_{41}(s^{-1})\} = \{26.23 \pm 0.67\} - \{(16730 \pm 820)/T(K)\} \quad (7)$$

where the uncertainties are at the 2σ (95.4%) confidence level. This yields an apparent activation energy of 139 ± 7 kJ/mol, essentially the same as the 144 kJ/mol enthalpy change for reaction 41. Glänzer et al. took data over the pressure range of 250 to 1420 kPa, while the pressure for our data ranges from 110 to 233 kPa. Pressure variation has no marked effect over this limited range. Therefore, it seems reasonable to assume that all of the conditions were near the high-pressure limit for azomethane dissociation.

The apparent activation energy suggests that the thermal decomposition might proceed by a concerted, nearly simultaneous, elimination of two methyl radicals. Both the activation energy and the prefactor, 2.4 × 10^{11} s^{-1}, are lower than the values expected for a sequential mechanism, where the first step of breaking one H_3C-N bond will require at least 209 kJ/mol (25 000 K/molecule), followed by later elimination of the second CH_3 from the unstable $H_3CN{=}N$ fragment. Direct evidence for concerted photoinitiated (351 nm) decomposition of azomethane has been demonstrated by North et al.,[63] although in their experiment the photons supply substantial excess energy. While the possibility of a thermal concerted reaction is intriguing, because of the data scatter and the limited range of pressures studied, we cannot rule out the possibility that the low apparent value of E_{act} could result from falloff behavior in a sequential mechanism. The points of Figure 5 are fit equally well, for example, by an expression of the form

$$\ln\{k_{41}(s^{-1})\} = \{90.6 \pm 5.0\} - \{7.99 \pm 0.71\} \ln T - \{25920/T(K)\} \quad (8)$$

which shows a small amount of curvature. Again, the uncertainties are at the 2σ (95.4%) confidence level. In this fit, the coefficient E_{act}/R was fixed while the other two were adjusted. This fixed value corresponds to an "E_{act}" of 215 kJ/mol, the C−N bond energy plus a small energy barrier.[63] Further experimental work is required to obtain a clear answer regarding the thermal decomposition mechanism for azomethane.

C. Rate of Methyl−Methyl Recombination. In Figure 6, our results for methyl−methyl recombination at 1.2 atm are compared to previous results obtained with shock tubes. The result of Glänzer et al. at 1350 K falls within the experimental errors of both sets of measurements. The result of Zaslonko and Smirnov at 1740 K is a factor of 7 high. We do not know the reason for this discrepancy. To compare our results to the measurements of Hwang et al., we use their Figure 5 and extrapolate to our higher pressure. We only present results at 1480, 1550, and 1700 K because to extrapolate their results at 1330 K requires that we move to a density beyond the boundary of their figure. The point at 1480 K is in very good agreement with our results. The two higher temperature points are slightly high. We note that Hwang et al. used a temperature-independent cross section for optical absorption when they simultaneously reduced all of their data with a regression analysis based upon a factorial design. From Table 2 we see that the correlation coefficient between the cross section and the rate coefficient for recombination is positive. Therefore, had they used a temperature-dependent cross section, similar in behavior to the results shown in Figure 4, they would have obtained lower rate coefficients at 1550 and 1700 K. This correction would bring the two data sets into even better agreement. We have not compared our results to the work of Clark et al. or of Held et al. since their measurements were performed at pressures a factor of 10 below our pressures. Extrapolations of their data to our experimental conditions are not justified.

VI. Conclusions

We have demonstrated that the tunable-laser flash-absorption technique can be used to accurately measure the kinetic behavior of the methyl radical under conditions where the chemistry is very fast. All of the kinetic information presented here was extracted from absorption profiles with a duration of less than 15 μs in the laboratory. With this approach we have provided new information on the cross section for absorption by the methyl radical and measured the rate of methyl−methyl recombination in the pressure region near one atmosphere and the important combustion temperature range 1100−1800 K. The previous results of Glänzer et al. and Hwang et al. are in complete agreement with the results presented here. These results will be used in a subsequent paper to determine the temperature-dependent behavior of the high-pressure rate coefficient and to perform global fits with several different expressions for the pressure-dependent behavior in the falloff region.

Acknowledgment. We wish to thank Chris C. Walker, an undergraduate student from Earlham College, for help with the analysis of the experimental profiles. He participated in the Fall 1993 and Winter 1994 Science and Engineering Research Semester programs. We thank D. F. Davidson, M. Di Rosa, E. J. Chang, and R. K. Hanson for giving us the unpublished preliminary values from their reevaluation of the cross section for optical absorption of the methyl radical and K. P. Lim and J. V. Michael for a copy of their unpublished manuscript on the methyl radical. We would like to acknowledge helpful discussions with J. V. Michael, R. G. McDonald, and A. F. Wagner. We thank J. Troe for helpful comments. This work was supported by the U.S. Department of Energy, Office of Basic Energy Sciences, Division of Chemical Sciences.

References and Notes

(1) Warnatz, J. In *Combustion Chemistry*; Gardiner, W. C., Jr., Ed.; Springer-Verlag: New York, 1984; p 197.
(2) Westbrook, C. K.; Dryer, F. L. *Prog. Energy Combust. Sci.* **1984**, *10*, 1.
(3) Kerr, J. A.; Moss, S. J. In *CRC Handbook of Bimolecular and Termolecular Gas Reactions* CRC Press: Cleveland, OH, 1981.
(4) Wardlaw, D. M.; Marcus, R. A. In *Evolution of Size Effects in Chemical Dynamics Part 1*; Prigogine, I., Rice, S. A., Eds.; John Wiley & Sons: New York, 1988; Vol. 70, p 231.
(5) Troe, J. *Combust. Flame* **1989**, *78*, 59.
(6) Mallard, W. G. NIST Chemical Kinetics Database, 1992.
(7) Hippler, H.; Luther, K.; Ravishankara, A. R.; Troe, J. *Z. Phys. Chem. NF (Frankfurt)* **1984**, *142*, 1.
(8) Slagle, I. R.; Gutman, D.; Davies, J. W.; Pilling, M. J. *J. Phys. Chem.* **1988**, *92*, 2455.
(9) Walter, D.; Grotheer, H.-H.; Davies, J. W.; Pilling, M. J.; Wagner, A. F. In *Twenty-Third Symp. (Int.) Combust.*; The Combustion Institute: Seattle, 1990; p 107.
(10) Clark, T. C.; Izod, T. P. J.; Kistiakowsky, G. B. *J. Chem. Phys.* **1971**, *54*, 1295.
(11) Held, A. M.; Manthorne, K. C.; Pacey, P. D.; Reinholdt, H. P. *Can. J. Chem.* **1977**, *55*, 4128.
(12) Glänzer, K.; Quack, M.; Troe, J. *Chem. Phys. Lett.* **1976**, *39*, 304.
(13) Glänzer, K.; Quack, M.; Troe, J. In *Sixteenth Symp. (Int.) Combust.*; The Combustion Institute: Seattle, 1977; p 949.
(14) van den Berg, H. E.; Callear, A. B.; Norstrom, R. J. *Chem. Phys. Lett.* **1969**, *4*, 101.
(15) Basco, N.; James, D. G. L.; Suart, R. D. *Int. J. Chem. Kinet.* **1970**, *2*, 215.
(16) Hwang, S. M.; Wagner, H. G.; Wolff, T. In *Twenty-Third Symp. (Int.) Combust.*; The Combustion Institute: Seattle, 1990; p 99.
(17) Zaslonko, I. S.; Smirnov, V. N. *Kinet. Catal.* **1979**, *20*, 575.
(18) Hwang, S. M.; Rabinowitz, M. J.; Gardiner Jr., W. C. *Chem. Phys. Lett.* **1993**, *205*, 157.
(19) Hessler, J. P.; Ogren, P. J. *J. Phys. Chem.*, following paper in this issue.
(20) Renaud, R.; Leitch, L. *Can. J. Chem.* **1954**, *32*, 545.
(21) Du, H.; Hessler, J. P. *J. Chem. Phys.* **1992**, *96*, 1077.
(22) Mirels, H. *Phys. Fluids* **1963**, *6*, 1201.
(23) VonDrasek, W. A.; Okajima, S.; Kiefer, J. H.; Ogren, P. J.; Hessler, J. P. *Appl. Opt.* **1990**, *29*, 4899.
(24) Herzberg, G.; Shoosmith, J. *Can. J. Phys.* **1956**, *34*, 523.
(25) Davidson, D. F.; Di Rosa, M. D. D.; Hanson, R. K.; Bowman, C. T. *Int. J. Chem. Kinet.* **1993**, *25*, 969.
(26) Frenklach, M.; Wang, H.; Rabinowitz, M. J. *Prog. Energy Combust. Sci.* **1992**, *18*, 47.
(27) Baulch, D. L.; Cobos, C. J.; Cox, R. A.; Esser, C.; Frank, P.; Just, T.; Kerr, J. A.; Pilling, M. J.; Troe, J.; Walker, R. W.; Warnatz, J. *J. Phys. Chem. Ref. Data* **1992**, *21*, 411.
(28) Tsang, W.; Hampson, R. F. *J. Phys. Chem. Ref. Data* **1986**, *15*, 1087.
(29) Michael, J. V.; Lim, K. P. in *Annual Review of Physical Chemistry*; Leone, S. R., Ed.; Annual Reviews Inc.: Palo Alto, CA, 1993; Vol. 44, p 429.
(30) Kee, R. J.; Rupley, F. M.; Miller, J. A. *The CHEMKIN Thermodynamic Data Base*; Sandia National Laboratories: 1987.
(31) Pamidimukkala, K. M.; Rogers, D.; Skinner, G. B. *J. Phys. Chem. Ref. Data* **1982**, *11*, 83.
(32) Dobis, O.; Benson, S. W. *Int. J. Chem. Kinet.* **1987**, *19*, 691.
(33) Russell, J. J.; Seetula, J. A.; Senkan, S. M.; Gutman, D. *Int. J. Chem. Kinet.* **1988**, *20*, 759.
(34) Myerson, A. L.; Thompson, H. M.; Joseph, P. J. *J. Chem. Phys.* **1965**, *42*, 3331.
(35) Lim, K. P.; Michael, J. V. In *Twenty-Fifth Symp. (Int.) Combustion*; The Combustion Institute: Seattle, in press.
(36) Frank, P. In *15th Int. Symp. Rarefied Gas Dynam.*; Grado, Italy, 1986; p 422.
(37) Frank, P.; Braun-Unkhoff, M. In *Complex Chemical Reaction Systems*; Warnatz, J., Jaeger, W., Eds.; Springer-Verlag: Berlin, 1987; Vol. 47, p 69.
(38) Gardiner, W. C., Jr.; Owen, J. H.; Clark, T. C.; Dove, J. E.; Bauer, S. H.; Miller, J. A.; McLean, W. J. In *Fifteenth Symp. (Int.) Combust.*; The Combustion Institute: Seattle, 1975; p 857.
(39) Kern, R. D.; Singh, H. J.; Wu, C. H. *Int. J. Chem. Kinet.* **1988**, *20*, 731.
(40) Hidaka, Y.; Nakamura, T.; Tanaka, H.; Inami, K.; Kawano, H. *Int. J. Chem. Kinet.* **1990**, *22*, 701.
(41) Gordon, M. S.; Truong, T. N.; Pople, J. A. *Chem. Phys. Lett.* **1986**, *130*, 245.
(42) Böhland, T.; Dobe, S.; Temps, F.; Wagner, H. G. *Ber. Bunsen-Ges. Phys. Chem.* **1985**, *89*, 1110.
(43) Böhland, T.; Temps, F.; Wagner, H. G. *Ber. Bunsen-Ges. Phys. Chem.* **1985**, *89*, 1013.
(44) Hanning-Lee, M. A.; Green, N. J. B.; Pilling, M. J.; Robertson, S. H. *J. Phys. Chem.* **1993**, *97*, 860.
(45) Feng, Y.; Niiranen, J. T.; Bencsura, A.; Knyazev, V. D.; Gutman, D.; Tsang, W. *J. Phys. Chem.* **1993**, *97*, 871.

(46) Gilbert, R. G.; Luther, K.; Troe, J. *Ber. Bunsen-Ges. Phys. Chem.* **1983**, *87*, 169.
(47) Möller, W.; Mozzhukhin, E.; Wagner, H. G. *Ber. Bunsen-Ges. Phys. Chem.* **1986**, *90*, 854.
(48) Pilling, M. J. in *Modern Gas Kinetics*; Pilling, M. J., Smith, I. W. M., Eds.; Blackwell Scientific Publications: Oxford, 1987; p 303.
(49) Ogren, P. J.; Hessler, J. P. *Int. J. Chem. Kinet.* **1995**, *27*, 719.
(50) Lutz, A. E.; Kee, R. J.; Miller, J. A. *SENKIN: A Fortran Program for Predicting Homogeneous Gas Phase Chemical Kinetics with Sensitivity Coefficients*; Sandia National Laboratories, 1987.
(51) Hessler, J. P.; Ogren, P. J. *J. Chem. Phys.* **1992**, *97*, 6249.
(52) Press, W. H.; Flannery, B. P.; Teukolsky, S. A.; Vetterling, W. T. in *Numerical Recipes The Art of Scientific Computing*; Cambridge University Press: New York, 1989; p 498.
(53) Hessler, J. P.; Current, D. H.; Ogren, P. J. *Comput. Phys.*, in press.
(54) Mitchell, R. E.; Kee, R. J. *A General-Purpose Computer Code for Predicting Chemical Kinetic Behavior Behind Incident and Reflected Shocks*, Sandia Report No. SAND89-8205, Mar 1982.
(55) Koike, T.; Morinaga, K. *Bull. Chem. Soc. Jpn.* **1981**, *54*, 530.
(56) Gardiner Jr, W. C.; Hwang, S. M.; Rabinowitz, M. J. *Energy Fuels* **1987**, *1*, 545.
(57) Wagner, A. F.; Wardlaw, D. M. *J. Phys. Chem.* **1988**, *92*, 2462.
(58) Laidler, K. J. In *Chemical Kinetics*; Harper & Row: New York, 1987; p 18.
(59) Davidson, D. F.; Chang, A. Y.; Di Rosa, M. D. D.; Hanson, R. K. *J. Quantum Spectrosc. Radiat. Transfer* **1993**, *49*, 559.
(60) Davidson, D. F.; Di Rosa, M. D. D.; Chang, E. J.; Hanson, R. K. *J. Quantum Spectrosc. Radiat. Transfer* **1995**, *53*, 581.
(61) Blass, W. E.; Halsey, G. W. *Deconvolution of Absorption Spectra*; Academic Press: New York, 1981.
(62) Jansson, P. A. *Deconvolution With Applications in Spectroscopy*; Academic Press, Inc.: New York, 1984.
(63) North, S. W.; Longfellow, C. A.; Lee, Y. T. *J. Chem. Phys.* **1993**, *99*, 4423.

JP951217W